ChemPubSoc Europe
DOI: 10.1002/ejic.201600201
EurJIC European Journal of Inorganic Chemistry
Full Paper

MOFs and Sensors

A Three-Dimensional Tetraphenylethene-Based Metal–Organic Framework for Selective Gas Separation and Luminescence Sensing of Metal Ions

Wei Yang,[a] Ganggang Chang,[a] Hailong Wang,*[a] Tong-Liang Hu,[a] Zizhu Yao,[b]
Khalid Alfooty,[c] Shengchang Xiang,[b] and Banglin Chen*[a,c]

Abstract: A three-dimensional porous metal–organic framework (MOF), UTSA-86, made up of cadmium ions and a chromophoric tetraphenylethene-based tetracarboxylate ligand, 4′,4′′′,4′′′′′,4′′′′′′′-(ethene-1,1,2,2-tetrayl)tetrakis(1,1′-biphenyl-4-carboxylic acid) (H_4ettc), has been synthesized and characterized by single-crystal X-ray diffraction analysis. This multifunctional MOF exhibits permanent porosity, selective gas uptake, and luminescence sensing of metal ions.

Introduction

Metal–organic frameworks (MOFs) or porous coordination polymers (PCPs) are the most brilliant representatives of inorganic–organic hybrid porous solids.[1,2] These new crystalline materials are constructed by the self-assembly of suitable metal ions/clusters and organic spacers; they therefore possess properties originating from both inorganic and organic components. Thus far, versatile applications of MOFs and porous CPs have been discovered, including gas storage and separation,[3] catalysis,[4] sensing,[5] and electronic devices.[6] New building blocks, that is, functional organic ligands and metal ions or clusters, have been developed to prepare new MOFs or porous CPs to further understand and extend their chemistry.[7] In theory it seems that an infinite number of MOFs and porous CPs are available by the self-assembly of metal ions/clusters and organic linkers by varying the reaction conditions, and the range of functions of porous MOFs and CPs no doubt will be greatly extended. Nevertheless, the practical demands of these functions have introduced further challenges, such as thermal/chemical stability, sensitivity, selectivity, and processability, on the way to real applications[8] that require extensive research endeavors to comprehend structure–property relationships in detail. Thus, it is very important to target special MOFs based on functional organic linkers and metal/clusters.

Given the fact that tetraphenylethene-based cores are very important functional components for the preparation of functional materials,[9] we chose the tetraphenylethene-based organic linker 4′,4′′′,4′′′′′,4′′′′′′′-(ethene-1,1,2,2-tetrayl)tetrakis(1,1′-biphenyl-4-carboxylic acid), (H_4ettc; see Scheme S1 in the Supporting Information) for assembly with $Cd(NO_3)_2{\cdot}4H_2O$, which produced the new porous MOF $[Cd_3(ettc)_{1.5}(H_2O)_2(dmf)]_n{\cdot}(dmf)_{12n}$ (UTSA-86). Single-crystal X-ray diffraction analysis illustrated that chains of cadmium are linked by the ettc tetracarboxylates in the crystal structure of UTSA-86, generating a three-dimensional (3D) porous MOF. This new functional MOF, which has both microporous and chromophoric character, exhibits moderately high selectivities for CO_2/CH_4 and CO_2/N_2 gas separation at room temperature and luminescence sensing of the Cu^{2+} and Zn^{2+} ions.

Results and Discussion

Crystal Structure of UTSA-86

UTSA-86 was synthesized by the solvothermal reaction between cadmium nitrate and H_4ettc in the presence of dmf as solvent at 80 °C. Single-crystal X-ray diffraction analysis revealed that UTSA-86 crystallizes in the orthorhombic system and belongs to the *Pmna* space group. As can be seen in Figure 1 (a,b), there are two kinds of ettc ligands in UTSA-86: One is named $ettc^{i}$ (Figure 1, a) and has four carboxylic groups exhibiting two different μ_2-η^1-η^1 coordination modes (*syn-syn* and *syn-trans* modes) and the other, $ettc^{ii}$, has four carboxylic groups showing μ_2-η^2-η^1-linking modes (Figure 1, b). In addition, there are two crystallographically independent, six-coordinate Cd ions with different coordination environments (Figure 1, c,d). For the Cd1 ion, the coordination sphere is completed by four oxygen atoms of ettc ligands, one oxygen atom of a water molecule, and one oxygen atom of the dmf molecule. The coordination polyhedron of the Cd2 ion is constructed of two oxygen atoms

---

[a] Department of Chemistry, University of Texas at San Antonio, One UTSA Circle, San Antonio, Texas 78249-0698, USA
E-mail: hailong.wang@utsa.edu
banglin.chen@utsa.edu
http://www.utsa.edu/chem/faculty/BanglinChen.html
[b] College of Material Science and Engineering, Fujian Provincial Key Laboratory of Polymer Materials, Fujian Normal University, 32 Shangsan Road, Fuzhou 350007, P. R. China
[c] Department of Chemistry, Faculty of Science, King Abdulaziz University, Jeddah 22254, Saudi Arabia

Supporting information for this article is available on the WWW under http://dx.doi.org/10.1002/ejic.201600201.

of two μ_2-η^1-η^1-coordinated carboxylic groups and four oxygen atoms of two carboxylic groups in the μ_2-η^2-η^1 coordination mode.

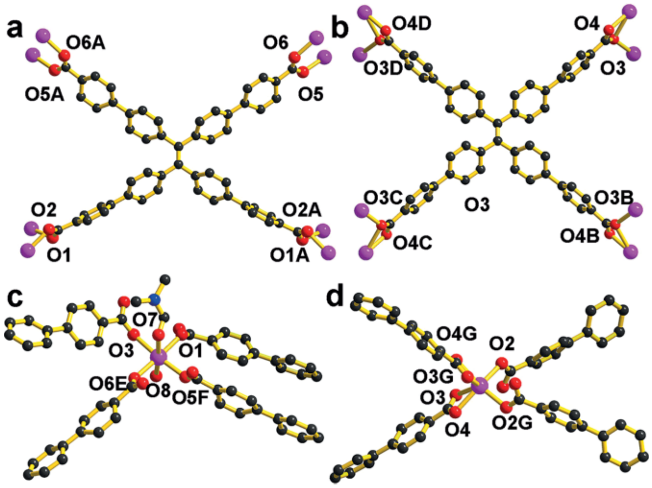

Figure 1. X-ray crystal structure of UTSA-86 showing the coordination conformations of a) ettc^i and b) ettc^{ii} and the coordination geometries of c) the Cd1 atom and d) the Cd2 atom (C: black; Cd: purple; N: blue; O: red). All hydrogen atoms have been omitted for clarity. Symmetry codes, A: 1 – *x*, *y*, *z*; B: *x*, 1 – *y*, *z*; C: –*x*, 1 – *y*, 1 – *z*; D: –*x*, *y*, *z*; E: –0.5 + *x*, *y*, 0.5 + *z*; F: 1 – *x*, –*y*, –*z*; G: *x*, 1 – *y*, –*z*.

In the crystal structure, the two kinds of Cd ions are bridged by ettc^i ligands to afford a 3D porous framework (see Figure S1a in the Supporting Information). The connection between the Cd ions and ettc^{ii} linkers yields an infinite 1D ribbon chain (see Figure S1b). Integration of the two kinds of Cd ions and ettc ligands leads to a 3D porous architecture with a very large pore size (ca. 8.0 × 14.4 Å) along the *b* axis (Figure 2, a). In contrast, a microporous structure is observed along the *c* and *a* axes with small pore sizes of around 5.1 and 4.1 Å, respectively (Figure 2, b and Figure S1c). The pore volume of 7023.2 Å^3 of UTSA-86, without taking into consideration any solvent molecules, was calculated by using the PLATON[10] software, and corresponds to a void of around 54 % per unit cell.

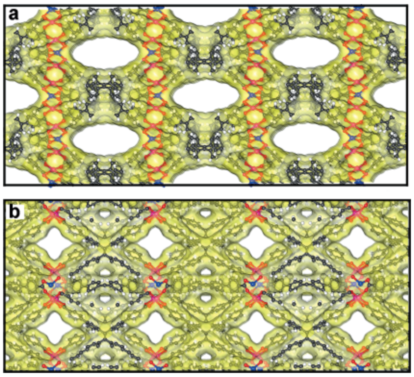

Figure 2. Packings diagram of the X-ray crystal structure of UTSA-86 along a)the *b* axis and b) the *c* axis. The pore surfaces of the channels are highlighted as yellow/grey (inner/outer) curved planes (C: black; Cd1: purple; Cd2: blue; O: red). All solvent moelculea have been omitted for clarity,.

Powder X-ray Diffraction Pattern and TGA Curve of UTSA-86

The phase purity of the material in the bulk was confirmed by elemental analysis and powder X-ray diffraction (PXRD; see Figure S2). Thermogravimetric analysis (TGA) revealed that the H_2O and dmf molecules of UTSA-86, whether in the guest or coordinated form, were gradually lost (obsd. 39.2 %, calcd. 38.9 %) in the temperature range of 25 to 205 °C (Figure 3). The organic spacer of this compound decomposed between 250 and 600 °C, resulting in a residue of CdO (obsd. 15.1 %, calcd. 15.2 %).

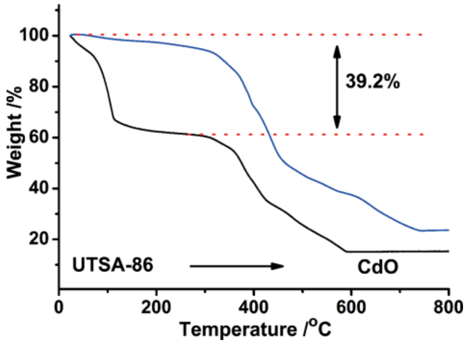

Figure 3. TGA curves of UTSA-86 (black line) and the desolvated UTSA-86a (blue line) in the range 25–800 °C under N_2.

Gas Sorption Behavior

To the best of our knowledge, owing to the high coordination number and large ionic radius of the cadmium ion, it is difficult to obtain permanently porous MOFs by the self-assembly of cadmium ions and organic ligands.[11] The UTSA-86 MOF possesses very large pores, which encouraged us to examine its porosity. After the activation of acetone-exchanged crystals of UTSA-86 under high vacuum at 393 K, a desolvated MOF (UTSA-86a) was produced. The TGA curve of this compound reveals that the coordinated H_2O molecules and solvent dmf guests of UTSA-86 were released completely during the activation process, as shown in Figure 3. In addition, the PXRD analysis manifested UTSA-86a to be highly crystalline. The activated UTSA-86a, with an absence of solvent molecules in the pores, exhibits a slightly different phase to that of the as-synthesized species (see Figure S2 in the Supporting Information); the CO_2 gas sorption isotherm at 196 K clearly illustrates its microporous nature (see Figure S3). The Brunauer–Emmett–Teller (BET) surface area of UTSA-86a was calculated to be 114 m^2 g^{-1}, and the pore volume measured from the CO_2 sorption is 0.11 cm^3 g^{-1}, which is markedly lower than that estimated from the single-crystal structure. This may be because the host framework is flexible, and only some pores have been opened by CO_2 molecules.

The CO_2, CH_4, and N_2 gas sorption isotherms were also measured at different temperatures to check the porosity and potential of UTSA-86a for gas separation; the results are shown in Figure 4. UTSA-86a takes up moderate amounts of carbon dioxide (33.0 and 19.2 cm^3 g^{-1} at 273 and 296 K, respectively), thereby further confirming the permanent porosity of this activated MOF. The coverage-dependent adsorption enthalpy of UTSA-86a with respect to the CO_2 molecule was calculated by using the virial method to improve the understanding of CO_2 sorption behavior (see Figure S4 in the Supporting Information). The enthalpy of adsorption at zero coverage of UTSA-86a is 25.0 kJ mol^{-1} for CO_2, which is even comparable with some MOFs with open metal sites, such as HKUST-1 (26 kJ mol^{-1})[12] and PCN-11 (23 kJ mol^{-1}).[12] Compared with the uptake of CO_2, UTSA-86a adsorbs smaller amounts of methane (7.9 and 4.9 $cm^3\,g^{-1}$) and nitrogen (5.1 and 1.8 $cm^3\,g^{-1}$) at 273 and 296 K, respectively, and 1 atm, and the enthalpies at zero coverage of UTSA-86a are 14.4 and 10.1 kJ/mol for CH_4 and N_2, respectively. The clearly different gas uptakes and enthalpies for CO_2, CH_4, or N_2 confirm the different affinities of UTSA-86a for these gas substrates, which shows the potential capacity of this new MOF for the selective separation of CO_2/N_2 and CO_2/CH_4.

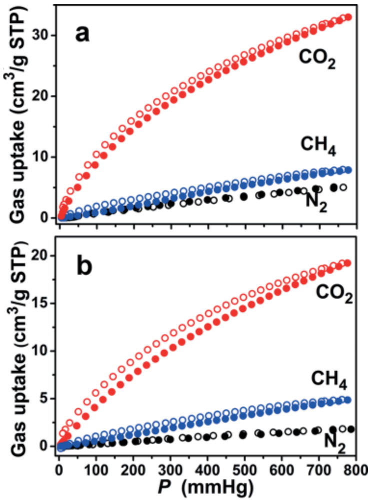

Figure 4. CO_2 (red), CH_4 (blue), and N_2 (black) sorption isotherms of UTSA-86a at a) 273 and b) 296 K (solid symbols: adsorption; open symbols: desorption).

Gas separation is of particular interest when exploring the functionalities of MOFs as they are very useful for obtaining highly pure gases in industry. We have therefore also been very interested in the use of porous MOF materials for gas separation.[13–16] Currently, it is very popular to deduce the selectivity of MOFs towards binary gas mixtures by utilizing the well-known ideal adsorbed solution theory (IAST) calculation[17] with the help of the dual-site Langmuir–Freundlich (DSLF) model.[18] By using the IAST method, we calculated the adsorption isotherms and selectivities for CO_2/CH_4 (50:50) and CO_2/N_2 (15:85) at different pressures and temperatures. The pressure-independent mixed-gas isotherms and selectivities for this activated MOF are shown in Figure 5 and Figures S5 and S6 in the Supporting Information. The gas selectivities were determined to be 11.3 and 7.1 for CO_2/CH_4 and 17.8 and 24.2 for CO_2/N_2 at 273 and 296 K, respectively. Selective CO_2 uptake is very useful for the purification of natural and flue gases. The selectivity for CO_2/CH_4 separation by adsorption is 11.3 at 273 K, which is comparable to the high values reported for other microporous MOF materials under similar conditions, including Tb(BCB) (ca. 4.1),[19] La(BTB) (ca. 6.4),[20] and InOF-14 (ca. 3.1).[21] In addition, to model the typical composition of flue gas mixtures from power plants, the calculated selectivities for CO_2/N_2 (15:85) span the range of 24.6–35.1 at 296 K, which indicates the potential of UTSA-86a as a promising adsorbent in the real process of CO_2/N_2 separation.

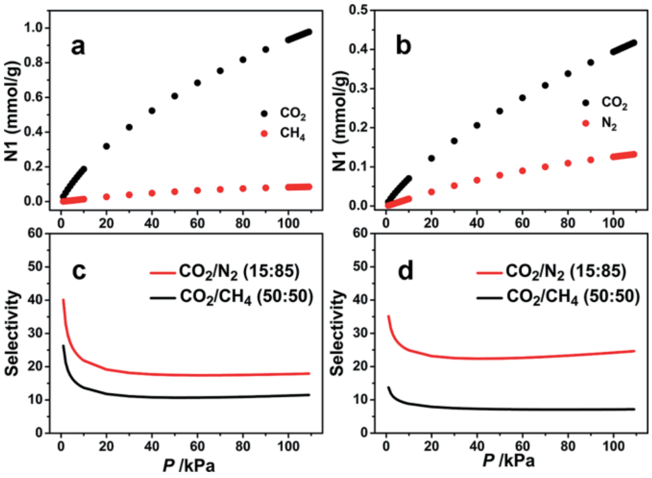

Figure 5. Mixture adsorption isotherms and adsorption selectivities of UTSA-86a for CO_2/CH_4 (50:50) and CO_2/CH_4 (15:85) at a–c) 273 K and d) 296 K as predicted by IAST.

Luminescence Sensing of Different Metals

The combination of TPE-based ligands and suitable metal ions, such as d^{10} ions, is a good strategy for constructing photoluminescent materials. The luminescent properties of TPE-based MOFs are very interesting because of their very high quantum yields and thus various applications in light-emitting devices and chemical sensors.[22,23] As a consequence, we studied the luminescent properties of H_4ettc and the complex UTSA-86 in the solid state at room temperature. The luminescence spectrum of the free H_4ettc ligand displays an emission maximum at 522 nm (λ_{ex} = 350 nm). This is typical of intraligand transitions, based on previous reports in the literature.[24a] After the self-assembly of Cd and the H_4TTC ligand, a clear blueshift of the emission is observed, with a maximum at 472 nm (λ_{ex} = 350 nm) in the luminescence spectrum of UTSA-86 (see Figure S7 in the Supporting Information), which is associated with an aggregate-induced effect (AIE).[24] This phenomenon is usually observed for tetraphenylethene-based MOFs.[25] It should be noted that the intraligand luminescence of TPE-based ligands is very sensitive to molecular conformation, aggregation state, and the coordinated metal species.[26] In addition, turn-on luminescence is often observed in TPE-based sensors.[25] These characteristics enable TPE-based MOFs to sensitively distinguish different chemicals and thus be very good candidates for chemical sensing. After the immersion of UTSA-86 crystals in dmf solutions containing $M(NO_3)_x \cdot nH_2O$ (M = Na^+, Ag^+, Cu^{2+}, Mg^{2+}, Zn^{2+}, Mn^{2+}, Co^{2+}, Ni^{2+}, Ca^{2+}, and Cr^{3+}) at a concentration of 1.0×10^{-2} M, the luminescence of the treated UTSA-86 was measured to investigate the potential of UTSA-86 for the luminescence sensing of different metals.

The various metal ions clearly show different influences on the luminescence of UTSA-86 (Figure 6). With zinc nitrate, the emission of the treated UTSA-86 exhibits a redshifted (15 nm) emission with a maximum at 487 nm and an enhanced intensity compared with the original crystals. In contrast, no significant spectral shifts were observed for UTSA-86 treated with other metal nitrate solutions. However, all the paramagnetic metals (Cu^{2+}, Mn^{2+}, Co^{2+}, Ni^{2+}, and Cr^{3+}) induced a decrease in the luminescence intensity at 472 nm. In the presence of Cu^{2+}, 98 % of the luminescence intensity of UTSA-86 was quenched. The diamagnetic metals Na^+ and Mg^{2+} caused an enhanced and unchanged intensity of the processed UTSA-86, respectively, whereas both Ca^{2+} and Ag^+ caused a decrease in the emission intensity. It should be noted that samples treated with Zn^{2+} and Na^+ ions in dmf solution show turn-on luminescence phenomena with a shift in the emission wavelength and an enhancement in the luminescence intensity, respectively. The luminescence intensity at 472 nm of the latter sample is only moderately enhanced (19 %), which is not sensitive enough to be distinguished by the naked eye. These results indicate that UTSA-86 is able to selectively distinguish Zn^{2+} and Cu^{2+} ions from other metal ions based on the clear turn-on and quenching luminescence phenomena, respectively. To comprehend the sensing mechanism, we performed powder X-ray diffraction measurements on UTSA-86 samples treated with different metal ions (10^{-2} M) in dmf solution for 36 h. The PXRD patterns of the treated samples match well that of the as-synthesized UTSA-86 (see Figure S8 in the Supporting Information), which indicates that the structure of the framework is maintained. Furthermore, we investigated the crystal structure again. The Cd ions are located in different six-coordinate environments; such coordination polyhedrons are not stable as the coordination number of the Cd ion is usually greater than six.[27] As a consequence, cadmium may be easily replaced by other transition metals.[27] The differences observed in the luminescence may be due to ion exchange. As expected, a clear color change between the original UTSA-86 (slightly yellow) and the species immersed in Cu^{2+} solution (1.0×10^{-2} M; green) is observed (see Figure S9), which confirms that Cu ions are incorporated into the UTSA-86. Energy-dispersive X-ray (EDX) analysis further confirmed the presence of Cu ions within UTSA-86 (see Figures S10 and S11), and the replacement of around 50 % of the Cd^{2+} ions by Cu^{2+} ions was determined by elemental analysis. This quenching effect of Cu^{2+} is a normal phenomenon for MOF sensors. The Cu^{2+} ion has an unsaturated d^9 electron configuration with the low-lying electron levels made up of partially filled d orbitals. The d–d transitions between these levels are non-emissive and lead to strong re-absorption, which usually weakens or quenches the MOF luminescence.[5a] This is also true for the luminescence of samples treated with solutions of paramagnetic ions. In contrast, the different emission intensities and shifts in emission wavelengths of the sample after immersion in different diamagnetic metal solutions may be caused by the different intra- and/or intermolecular energy transfer in the ettc ligand(s). However, the specific mechanism is still not clear.

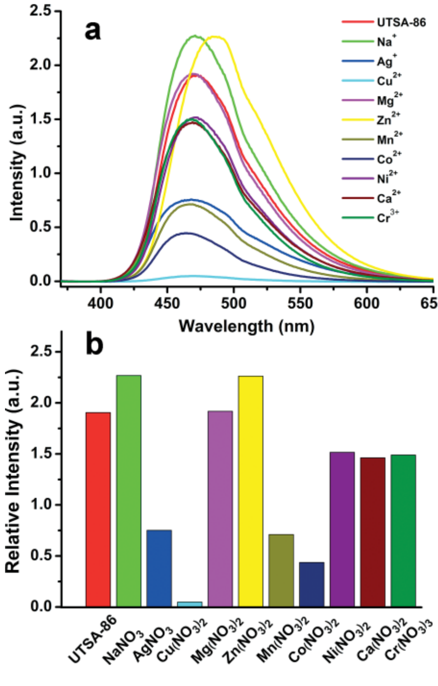

Figure 6. a) Emission spectra and b) photoluminescence intensities for complex UTSA-86 and samples of UTSA-86 treated with different metal ions (10^{-2} M) in dmf solution at room temperature for 36 h.

Conclusions

We have successfully prepared a new multifunctional metal–organic framework, UTSA-86. The activated species shows permanent porosity and moderately high selectivities for mixed CO_2/CH_4 and CO_2/N_2 gas separations, as predicted by IAST calculations. In addition, the MOF has potential applications in the chemical sensing of divalent Zn and Cu ions by means of the luminescence turn-on and quenching effect. We are now exploring the use of new functional carboxylic acids to synthesize further MOFs with multiple functions.

Experimental Section

General: All reagents and solvents were used as received from commercial suppliers without further purification. Tetrakis(4-bromophenyl)ethene was prepared according to the literature.[28] Tetramethyl-4′,4′′′,4′′′′′,4′′′′′′′-(ethene-1,1,2,2-tetrayl)tetrakis(1,1′-biphenyl-4-carboxylate) (Me_4ettc) and 4′,4′′′,4′′′′′,4′′′′′′′-(ethene-1,1,2,2-tetrayl)tetrakis(1,1′-biphenyl-4-carboxylic acid) (H_4ettc) were prepared according to slight modifications of the reported procedures (see Scheme S1 in the Supporting Information).[29] NMR spectra were recorded with a Varian INOVA 500 MHz spectrometer at room temperature. $CDCl_3$ (δ = 7.26 ppm) and [D_6]DMSO (δ = 2.50 ppm) were used as internal standards for the ^{1}H NMR spectra. The FTIR spectrum was recorded with a Bruker Vector 22 IR spectrometer at room temperature. Thermogravimetric analysis (TGA) was performed with a Shimadzu TGA-50 thermogravimetric analyzer under N_2 at a heating rate of 3 °C/min. Elemental analysis was performed with a Perkin–Elmer 240 CHN analyzer from Galbraith Laboratories. Steady-state fluorescence spectroscopic studies were performed with an Hitachi F 4500 instrument using a slit width of 5.0 nm for excitation and 2.5 nm for emission. The photomultiplier voltage was 700 V. Scanning electron microscope (SEM) was performed with a SIRION-100 instrument on a powder sample previously dried and sputtercoated with a thin layer of gold. Energy-dispersive X-ray spectroscopy (EDX) analysis was performed to confirm the presence of Cu^{II} and the replacement of Cd^{II} by Cu^{II}.

$[Cd_3(ettc)_{1.5}(H_2O)_2(dmf)]_n\cdot(dmf)_{12n}$ (UTSA-86): The starting materials $Cd(NO_3)_2\cdot4H_2O$ (0.15 g), H_4ettc (0.08 g), and dmf (5 mL) were sealed in a 23 mL vial, which was heated at 80 °C for 48 h. After being cooled to room temperature, the vial was cut open; slightly yellow crystals suitable for X-ray diffraction were obtained by filtration in a yield of 0.11 g, 43 % (based on H_4ettc ligand). IR (KBr): $\tilde{\nu}$ = 3031 (m), 1641 (m), 1574 (m), 1514 (s), 1374 (s), 985 (s), 823 (s), 760 (m) cm^{-1}. $C_{120}H_{143}Cd_3N_{13}O_{27}$: C 56.82, H 5.68, N 7.18; found C 56.78, H 5.63, N 7.17.

Single-Crystal X-ray Diffraction: Crystallographic data for a single crystal of UTSA-86 was collected with an Oxford Diffraction SuperNova diffractometer with Cu-K_α radiation (λ = 1.54184 Å) at 100.00(16) K. The final unit cell parameters were derived from global refinements of reflections obtained from the integration of all frame data. The collected frames were integrated by using the preliminary cell-orientation matrix. CrysAlisPro[30] software was used to collect the frames of data, index the reflections, and determine the lattice constants. SCALE3 ABSPACK software[30] was utilized for absorption correction. The structure was solved by direct methods (SHELXS-97) and refined by full-matrix least-squares methods on F^2 (SHELXL-97).[31] Anisotropic thermal parameters were used for the non-hydrogen atoms and isotropic parameters for the hydrogen atoms. Hydrogen atoms were added geometrically and refined by using a riding model. The "PART" restraint was used to deal with the disorder of the benzene ring in the ettc ligand. In addition, we note that the "SQUEEZE" command was employed because of the seriously disordered solvent molecules in the UTSA-86 pores. Selected crystallographic data and pertinent information for this compound are summarized in Table S1, and selected bond lengths and angles are listed in Table S2.

CCDC 1455687 (for UTSA-86) contains the supplementary crystallographic data for this paper. These data can be obtained free of charge from The Cambridge Crystallographic Data Centre.

Gas Sorption Measurements: Before the gas sorption measurements, as-synthesized crystals of UTSA-86 were exchanged with dry acetone six times and then evacuated at 6 µmmHg at 393 K to generate activated UTSA-86. Gas sorption data of activated UTSA-86 were collected by using a Micromeritics ASAP 2020 surface area analyzer; the measurement temperatures were maintained at 196, 273, and 296 K by using a bath of dry ice/acetone slurry, an ice/water mixture, and a water bath in an air-conditioned 23 °C laboratory, respectively.

IAST Calculations: The adsorption isotherms and gas selectivities of CO_2/CH_4 (50:50) and CO_2/N_2 (15:85) at 273 and 296 K were calculated based on the ideal adsorbed solution theory (IAST) proposed by Myers and Prausnitz,[17] The results are shown in Figure 5, Figures S5 and S6, and Table S3 in the Supporting Information. To weight the sorption performance of this MOF towards the separation of binary mixed gases, the parameters fitted from the single-component CO_2, CH_4, and N_2 adsorption isotherms based on the dual-site Langmuir–Freundlich (DSLF) model were used in the IAST calculations.[18] The fitting parameters of the DSLF equation are listed in Table S4.

Luminescence Sensing of UTSA-86**:** The luminescence of UTSA-86 was investigated in the solid state at room temperature and compared with that of H_4ettc. For the experiments involving the sensing metal ions, crystals of UTSA-86 (15 mg) were immersed in dmf solutions (20 mL) containing 1×10^{-2} M of $M(NO_3)_x\cdot nH_2O$ (M = Na^+, Ag^+, Cu^{2+}, Mg^{2+}, Zn^{2+}, Mn^{2+}, Co^{2+}, Ni^{2+}, Ca^{2+}, and Cr^{3+}). After immersion for 36 h, the treated crystals were filtered and their solid luminescence determined.

Acknowledgments

This work was supported by the Welch Foundation (grant number AX-1730, grant to B. C.).

Keywords: Metal–organic frameworks · Microporous materials · Gas separation · Luminescence · Sensors · Ligand design

[1] a) H. Furukawa, K. E. Cordova, M. O'Keeffe, O. M. Yaghi, *Science* **2013**, *341*, 974; b) J.-P. Zhang, Y.-B. Zhang, J.-B. Lin, X.-M. Chen, *Chem. Rev.* **2012**, *112*, 1001–1033; c) O. K. Farha, J. T. Hupp, *Acc. Chem. Res.* **2010**, *43*, 1166–1175; d) M. Li, D. Li, M. O'Keeffe, O. M. Yaghi, *Chem. Rev.* **2014**, *114*, 1343–1370; e) Y. Cui, B. Li, H. He, W. Zhou, B. Chen, G. Qian, *Acc. Chem. Res.* **2016**, *49*, 483–493.

[2] a) J. E. Mondloch, M. J. Katz, W. C. Isley III, P. Ghosh, P. Liao, W. Bury, G. W. Wagner, M. G. Hall, J. B. DeCoste, G. W. Peterson, R. Q. Snurr, C. J. Cramer, J. T. Hupp, O. K. Farha, *Nat. Mater.* **2015**, *14*, 512–516; b) Z. Zhang, H. T. H. Nguyen, S. A. Miller, S. M. Cohen, *Angew. Chem. Int. Ed.* **2015**, *54*, 6152–6157; *Angew. Chem.* **2015**, *127*, 6250; c) H. Wu, Y. S. Chua, V. Krungleviciute, M. Tyagi, P. Chen, T. Yildirim, W. Zhou, *J. Am. Chem. Soc.* **2013**, *135*, 10525; d) Q.-L. Zhu, Q. Xu, *Chem. Soc. Rev.* **2014**, *43*, 5468–5512.

[3] a) J.-R. Li, J. Sculley, H.-C. Zhou, *Chem. Rev.* **2012**, *112*, 869–932; b) H. Wu, Q. Gong, D. H. Olson, J. Li, *Chem. Rev.* **2012**, *112*, 836–868; c) H. Sato, W. Kosaka, R. Matsuda, A. Hori, Y. Hijikata, R. V. Belosludov, S. Sakaki, M. Takata, S. Kitagawa, *Science* **2014**, *343*, 167–170; d) R. Vaidhyanathan, S. S. Iremonger, G. K. H. Shimizu, P. G. Boyd, S. Alavi, T. K. Woo, *Science* **2010**, *330*, 650–653; e) C. Serre, C. Mellot-Draznieks, S. Surblé, N. Audebrand, Y. Filinchuk, G. Férey, *Science* **2007**, *315*, 1828–1831; f) P. Nugent, Y. Belmabkhout, S. D. Burd, A. J. Cairns, R. Luebke, K. Forrest, T. Pham, S. Ma, B. Space, L. Wojtas, M. Eddaoudi, M. J. Zaworotko, *Nature* **2013**, *495*, 80–84; g) K. A. Cychosz, A. G. Wong-Foy, A. J. Matzger, *J. Am. Chem. Soc.* **2009**, *131*, 14538–14543; h) B. Chen, S. Xiang, G. Qian, *Acc. Chem. Res.* **2010**, *43*, 1115–11124; i) K. Sumida, D. L. Rogow, J. A. Mason, T. M. McDonald, E. D. Bloch, Z. R. Herm, T.-H. Bae, J. R. Long, *Chem. Rev.* **2012**, *112*, 724–781.

[4] a) T. Zhang, W. Lin, *Chem. Soc. Rev.* **2014**, *43*, 5982–5993; b) J. Liu, L. Chen, H. Cui, J. Zhang, L. Zhang, C.-Y. Su, *Chem. Soc. Rev.* **2014**, *43*, 6011–6061; c) W.-Y. Gao, M. Chrzanowski, S. Ma, *Chem. Soc. Rev.* **2014**, *43*, 5841–5866; d) M. Zhao, S. Ou, C.-D. Wu, *Acc. Chem. Res.* **2014**, *47*, 1199–1207.

[5] a) Y. Cui, Y. Yue, G. Qian, B. Chen, *Chem. Rev.* **2012**, *112*, 1126–1162; b) L. E. Kreno, K. Leong, O. K. Farha, M. Allendorf, R. P. V. Duyne, J. T. Hupp, *Chem. Rev.* **2012**, *112*, 1105–1125; c) Z. Hu, B. J. Deibert, J. Li, *Chem. Soc. Rev.* **2014**, *43*, 5815–5840.

[6] a) J. Yu, Y. Cui, H. Xu, Y. Yang, Z. Wang, B. Chen, G. Qian, *Nat. Commun.* **2013**, *4*, 2719; b) P. Ramaswamy, N. E. Wong, G. K. H. Shimizu, *Chem. Soc. Rev.* **2014**, *43*, 5913–5932; c) V. Stavila, A. A. Talin, M. D. Allendorf, *Chem. Soc. Rev.* **2014**, *43*, 5994–6010; d) L. Sun, T. Miyakai, S. Seki, M. Dincă, *J. Am. Chem. Soc.* **2013**, *135*, 8185–8188.

[7] a) M. Eddaoudi, D. F. Sava, J. F. Eubank, K. Adil, V. Guillerm, *Chem. Soc. Rev.* **2015**, *44*, 228–249; b) Y. He, B. Li, M. O'Keeffe, B. Chen, *Chem. Soc. Rev.* **2014**, *43*, 5618–5656; c) W. Lu, Z. Wei, Z.-Y. Gu, T.-F. Liu, J. Park, J. Tian, M. Zhang, Q. Zhang, T. Gentle III, M. Bosch, H.-C. Zhou, *Chem. Soc. Rev.* **2014**, *43*, 5561–5593.

[8] a) A. G. Slater, A. I. Cooper, *Science* **2015**, *348*, aaa8075; b) N. C. Burtch, H. Jasuja, K. S. Walton, *Chem. Rev.* **2014**, *114*, 10575–10612.

[9] R. Hu, N. L. C. Leung, B.-Z. Tang, *Chem. Soc. Rev.* **2014**, *43*, 4494–4562.

[10] A. L. Spek, *PLATON, A Multipurpose Crystallographic Tool*, Utrecht University, The Netherlands, **2005**.

[11] a) H.-R. Fu, F. Wang, J. Zhang, *Dalton Trans.* **2014**, *43*, 4668–4673; b) Y. Chen, Z. Li, Q. Liu, Y. Shen, X. Wu, D. Xu, X. Ma, L. Wang, Q.-H. Chen, Z. Zhang, S. Xiang, *Cryst. Growth Des.* **2015**, *15*, 3847–3852; c) H. He, Y.

Song, C. Zhang, F. Sun, R. Yuan, Z. Bian, L. Gao, G. Zhu, *Chem. Commun.* **2015**, *51*, 9463–9466.

[12] J. M. Simmons, H. Wu, W. Zhou, T. Yildirim, *Energy Environ. Sci.* **2011**, *4*, 2177–2185.

[13] a) T. Hu, H. Wang, B. Li, R. Krishna, H. Wu, W. Zhou, Y. Zhao, Y. Han, X. Wang, W. Zhu, Z. Yao, S. Xiang, B. Chen, *Nature Commun.* **2015**, *6*, 7328; b) Y. Yue, J. Rabone, H. Liu, S. Mahurin, M. Li, H. Wang, Z. Lu, B. Chen, J. Wang, Y. Fang, S. Dai, *J. Phys. Chem. C* **2015**, *119*, 9442–9449; c) J. Yu, Y. Cui, C. Wu, Y. Yang, B. Chen, G. Qian, *J. Am. Chem. Soc.* **2015**, *137*, 4026.

[14] a) W. Yang, B. Li, H. Wang, O. Alduhaish, K. Alfooty, M. Zayed, P. Li, H. Arman, B. Chen, *Cryst. Growth Des.* **2015**, *15*, 2000–2004; b) P. Li, Y. He, Y. Zhao, L. Weng, H. Wang, R. Krishna, H. Wu, W. Zhou, M. O'Keeffe, Y. Han, B. Chen, *Angew. Chem. Int. Ed.* **2015**, *54*, 574–577; *Angew. Chem.* **2015**, *127*, 584; c) Z. Guo, D. Yan, H. Wang, D. Tesfagaber, X. Li, Y. Chen, W. Huang, B. Chen, *Inorg. Chem.* **2015**, *54*, 200–204.

[15] a) Y. Cui, F. Zhu, B. Chen, G. Qian, *Chem. Commun.* **2015**, *51*, 7420–7431; b) P. Li, H. Arman, H. Wang, L. Weng, K. Alfooty, R. F. Angawi, B. Chen, *Cryst. Growth Des.* **2015**, *15*, 1871–1875.

[16] a) H. Alawisi, B. Li, K. Alfooty, L. Wu, S. Xiang, H. Wang, B. Chen, *Inorg. Chem. Commun.* **2014**, 106–109; b) D. Yan, B. Chen, Q. Duan, *Inorg. Chem. Commun.* **2014**, 34–36.

[17] A. L. Myers, J. M. Prausnitz, *AIChE J.* **1965**, *11*, 121–127.

[18] D. Banerjee, Z. Zhang, A. Plonka, J. Li, J. Parise, *Cryst. Growth Des.* **2012**, *12*, 2162–2165.

[19] Z. Guo, X. Song, H. Lei, H. Wang, S. Su, H. Xu, G. Qian, H. Zhang, B. Chen, *Chem. Commun.* **2015**, 376–379.

[20] Z.-J. Lin, Y.-B. Huang, T.-F. Liu, X.-Y. Li, R. Cao, *Inorg. Chem.* **2013**, *52*, 3127–3132.

[21] J. Qian, Q. Li, L. Liang, Y. Yang, Z. Cao, P. Yu, S. Huang, M. Hong, *Chem. Commun.* **2016**, DOI: 10.1039/c5cc10359b.

[22] a) Q. Gong, Z. Hu, B. J. Deibert, T. J. Emge, S. J. Teat, D. Banerjee, B. Mussman, N. D. Rudd, J. Li, *J. Am. Chem. Soc.* **2014**, *136*, 16724–16727; b) Z. Hu, G. Huang, W. P. Lustig, F. Wang, H. Wang, S. J. Teat, D. Banerjee, D. Zhang, J. Li, *Chem. Commun.* **2015**, *51*, 3045–3048.

[23] a) N. B. Shustova, A. F. Cozzolino, S. Reineke, M. Baldo, M. Dincă, *J. Am. Chem. Soc.* **2013**, *135*, 13326–13329; b) Z. Hu, W. P. Lustig, J. Zhang, C. Zheng, H. Wang, S. J. Teat, Q. Gong, N. D. Rudd, J. Li, *J. Am. Chem. Soc.* **2015**, *137*, 16209–16215; c) M. Zhang, G. Feng, Z. Song, Y.-P. Zhou, H.-Y. Chao, D. Yuan, T. T. Y. Tan, Z. Guo, Z. Hu, B.-Z. Tang, B. Liu, D. Zhao, *J. Am. Chem. Soc.* **2014**, *136*, 7241–7244.

[24] a) Z. Wei, Z.-Y. Gu, R. K. Arvapally, Y.-P. Chen, R. N. McDougald Jr., J. F. Ivy, A. A. Yakovenko, D. Feng, M. A. Omary, H.-C. Zhou, *J. Am. Chem. Soc.* **2014**, *136*, 8269–8276; b) X. Wang, J. Hu, G. Zhang, S. Liu, *J. Am. Chem. Soc.* **2014**, *136*, 9890–9893.

[25] a) N. B. Shustova, B. D. McCarthy, M. Dincă, *J. Am. Chem. Soc.* **2011**, *133*, 20126–20129; b) N. B. Shustova, T.-C. Ong, A. F. Cozzolino, V. K. Michaelis, R. G. Griffin, M. Dincă, *J. Am. Chem. Soc.* **2012**, *134*, 15061–15070.

[26] a) J. Mei, N. L. C. Leung, R. T. K. Kwok, J. W. Y. Lam, B.-Z. Tang, *Chem. Rev.* **2015**, *115*, 11718–11940; b) J. Wang, J. Mei, R. Hu, J.-Z. Sun, A. Qin, B.-Z. Tang, *J. Am. Chem. Soc.* **2012**, *134*, 9956–9966.

[27] a) Z. Zhang, L. Wojtas, M. Eddaoudi, M. J. Zaworotko, *J. Am. Chem. Soc.* **2013**, *135*, 5982–5985; b) Z. Zhang, L. Zhang, L. Wojtas, P. Nugent, M. Eddaoudi, M. J. Zaworotko, *J. Am. Chem. Soc.* **2012**, *134*, 924–927.

[28] H. Wang, B. Li, H. Wu, T.-L. Hu, Z. Yao, W. Zhou, S. Xiang, B. Chen, *J. Am. Chem. Soc.* **2015**, *137*, 9963–9970.

[29] Q. Zhang, J. Su, D. Feng, Z. Wei, X. Zou, H.-C. Zhou, *J. Am. Chem. Soc.* **2015**, *137*, 10064–10067.

[30] *CrysAlisPro*, version 1.171.33.66, Oxford Diffraction Ltd., Abingdon, U. K., **2010**.

[31] G. M. Sheldrick, *Acta Crystallogr., Sect. A* **2008**, *64*, 112–122.

Received: February 27, 2016

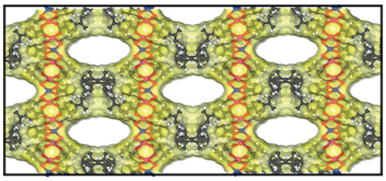

A three-dimensional multifunctional metal–organic framework (MOF), UTSA-86, made up of cadmium ions and a tetraphenylethene-based tetracarboxylate ligand has been synthesized and characterized by single-crystal X-ray diffraction analysis. This MOF exhibits permanent porosity, selective gas uptake, and luminescence sensing of metal ions.

DOI: 10.1002/ejic.201600201